



# CHORUS

This is the accepted manuscript made available via CHORUS. The article has been published as:

Local positional and spin symmetry breaking as a source of magnetism and insulation in paramagnetic  $\text{EuTi}_3\text{O}_7$

Oleksandr I. Malyi, Xin-Gang Zhao, Annette Bussmann-Holder, and Alex Zunger  
Phys. Rev. Materials **6**, 034604 — Published 28 March 2022

DOI: [10.1103/PhysRevMaterials.6.034604](https://doi.org/10.1103/PhysRevMaterials.6.034604)

# Local positional and spin symmetry breaking as a source of magnetism and insulation in paramagnetic $\text{EuTiO}_3$

Oleksandr I. Malyi<sup>1</sup>, Xin-Gang Zhao<sup>1</sup>, Annette Bussmann-Holder<sup>2</sup>, and Alex Zunger<sup>1,\*</sup>

<sup>1</sup>Renewable and Sustainable Energy Institute, University of Colorado, Boulder, Colorado 80309, USA

<sup>2</sup>Max-Planck-Institute for Solid State Research, Heisenbergstr. 1, Stuttgart, 70569, Germany

Email: [Alex.Zunger@Colorado.edu](mailto:Alex.Zunger@Colorado.edu)

## Abstract

We consider theoretically the paramagnetic phases of  $\text{EuTiO}_3$  that represent configurations created by two sets of microscopic degrees of freedom (m-DOF): positional symmetry breaking due to octahedral rotations and magnetic symmetry breaking due to spin disorder. The effect of these sets of m-DOFs on the electronic structure and properties of the para phases is assessed by considering sufficiently large (super) cells with the required nominal global average symmetry, allowing, however, the *local* positional and magnetic symmetries to be lowered. We find that tendencies for local symmetry breaking can be monitored by following total energy lowering in mean-field like density functional theory, without recourse for strong correlation effects. While most nominally cubic  $\text{ABO}_3$  perovskites are known for their symmetry breaking due to the B-atom sublattice, the case of f-electron magnetism in  $\text{EuTiO}_3$  is associated with A- sublattice symmetry breaking and its coupling to structural distortions. We find that (i) paramagnetic *cubic*  $\text{EuTiO}_3$  has an intrinsic tendency for both magnetic and positional symmetry breaking, while paramagnetic *tetragonal*  $\text{EuTiO}_3$  has only magnetic symmetry lowering and no noticeable positional symmetry lowering with respect to low-temperature antiferromagnetic tetragonal phase. (ii) Properly modeled paramagnetic tetragonal and cubic  $\text{EuTiO}_3$  have a nonzero local magnetic moment on each Eu ion, consistent with the experimental observations of local magnetism in the para phases of  $\text{EuTiO}_3$  significantly above the Néel temperature. Interestingly, (iii) the local positional distortion modes in the short-range ordered para phases are inherited from the long-range ordered low-temperature antiferromagnetic ground state phase.

## I. Introduction

ABO<sub>3</sub> oxide perovskites have attracted significant research interest largely because they represent the rich consequences of many possible configurational arrangements of a few basic microscopic degrees of freedom (m-DOF). The latter include *structural motifs* (rotated, tilted, deformed, or disproportionated BO<sub>6</sub> octahedra), *spin motifs* in magnetic configuration, and *dipole motifs* in a ferroelectric configuration. The low-temperature ordered structure of ABO<sub>3</sub> can be described theoretically with a sufficient number of m-DOFs needed to capture the *ordered polymorphs*, generally modestly small crystallographic, magnetic, or dipolar unit cells. However, the higher temperature para (elastic, magnetic, electric) phases, lacking long-range order, are inherently more complex and may require non-trivial unit cells that can accommodate the required m-DOFs. Here, we analyze theoretically the electronic and magnetic structure of the para phases of EuTiO<sub>3</sub> (ETO) studying positional symmetry breaking due to octahedral rotations and magnetic symmetry breaking due to spin disorder and their effects on the electronic and magnetic properties.

ETO containing an Eu<sup>2+</sup>(4f<sup>7</sup>) magnetic ion on the A- sublattice of the ABO<sub>3</sub> perovskite structure and a nonmagnetic Ti<sup>4+</sup>(d<sup>0</sup>) ion on the B-atom sublattice offers an interesting case of f-electron antiferro as well as para magnetism. ETO exhibits three principal phases confirmed by crystallographic and magnetic data[1-9] (Table I): below the Néel temperature  $T_N \sim 5.4 \pm 0.3$  K [6,7,10,11], ETO is in the  $\alpha$  phase which is an antiferromagnetic (AFM) insulator, classified crystallographically[6] as tetragonal (I4/mcm) space group. Between  $T_N$  and  $T_S = 282$  K, it is in the  $\beta$  phase being a paramagnetic (PM) tetragonal (I4/mcm) insulator[1-6,9], whereas at temperatures  $T > 282$  K, the  $\gamma$  phase is a paramagnetic cubic (Pm-3m) insulator.[1-6,9] Additional phase transitions were inferred within the temperature range assigned to the tetragonal  $\beta$  phase on the basis of the temperature-dependence of birefringence[11-13], X-ray diffraction (XRD) data[9],  $\mu$ SR experiments[9], and dielectric measurements[14]. Most of these observations were made under an applied magnetic field. A more recent XRD analysis of polycrystalline ETO on SrTiO<sub>3</sub> at 100 K without an applied magnetic field[9] showed no additional structural transition except those shown in Table I, in agreement with the analysis of pair distribution function[2,8] and other XRD analysis[1-8].

**Table I.** Summary of the three phases  $\alpha$ ,  $\beta$ , and  $\gamma$  of  $\text{EuTiO}_3$  in increasing order of temperatures, and their magnetic configuration with corresponding DFT calculations presented in this work. The information on the right-hand side describes the results of the current calculations, the existence of positional symmetry breaking in the form of octahedral tilting, and the ensuing formation of a polymorphous network; the type of symmetry distortion modes found in the calculation, the distribution of Eu magnetic moments, and the (generally underestimated) DFT band gap. Other literature DFT results are compared in the main text.

Experiment					Results of calculations in this work				
Phase name	Nominal crystal structure	Mag. config.	Temperature (K)	Exp. band gap (eV)	Octahed. tilting	Structural polym.	Distortion mode	Eu local magnetic moments	DFT band gap (eV)
$\gamma$	Pm-3m	PM	$T > 282$ [1-6,9]	0.8 [15] 0.93 [16] 1.32 [17] 4.53 [18]	yes	yes	$R_5^-, T_2, DT_5, M_2^+$	$6.88 \pm 0.005$	0.27
$\beta$	I4/mcm	PM	$\sim 5.4 < T < 282$ [1-6,9]	1.29 [17]	yes	no	$R_5^-$	$6.88 \pm 0.005$	0.31
$\alpha$	I4/mcm	AFM	$T < 5.4 \pm 0.3$ [6,7,10,11]	-	yes	no	$R_5^-$	6.88	0.33

*Different literature views on the nature of the microscopic structure of the PM configurations:* PM phases, in general, are defined by the lack of long-range order and having a total zero magnetization. The simplest conceptual realization of these conditions is that *each* site would have a zero moment. This initial view resulted in referring to paramagnetic phases as "*nonmagnetic*" or "*nominally nonmagnetic*".[11,14] Such a nonmagnetic interpretation of paramagnetism predicts, within the density functional theory (DFT) as will be illustrated below, a gapless electronic structure, in contradiction with diffuse reflectance spectra measured at room temperature of  $\text{EuTiO}_3$ , showing an insulating band gap of  $\sim 0.8$  eV.[15]

We note in passing that the scenario of describing a PM as a collection of nonmagnetic sites has been common in the band structure literature for d-electron perovskites[19-21] and binary d-electron oxides[22]. This view led to the well-known contradiction between the predicted (false) metallic character in PM oxides vs the observed insulating character, leading to the rise of the electron correlated view of Mott gapping as a solution of this contradiction.[23,24] However, it was recently demonstrated[25-30] that allowing for spatial and spin symmetry breaking leads to proper gapping even in the mean-field band theory.

A more advanced interpretation of the microscopic character of spin disordered PM phases (analogous to chemical disorder in alloys) has allowed non-zero local moments that are disordered in a specific way. For example, in the Disordered Local Moment (DLM) model[31-33] within the single-site (SS) coherent-potential approximation (CPA)[34] it was assumed that the moment and charge on a given site is independent of its local

1 environment, e.g., on how many spin up and how many spin down neighbors coordinate this site. This particular  
2 restriction in the CPA DLM leads to a picture that each local moment on a site is identical for all magnetic sites—  
3 neglecting charge and moment fluctuations. However, it was later noted that this particular version of a disorder  
4 underlying the site-coherent potential approximations leads incorrectly to vanishing electrostatic Madelung  
5 energy.[35,36] The realization that such models of disorder used to represent spin disorder in DLM or chemical  
6 disorder in random alloys are lacking, motivated more recently[35-37] a more general approach allowing the  
7 charge and moments on each site to depend on its local environment. This is possible by using a supercell or by  
8 a multi-site description, as will be discussed below, which allows the magnetic moment on Eu to always be finite  
9 and to depend on its local coordination environment.

10 In light of the above discussion of the different views on the microscopic nature of the disorder, we wish to  
11 focus on two interesting features in the para phases of ETO:

12 (a) *Magnetic activity in the PM phases:* Although the PM phases of ETO were often referred to as "*nonmagnetic*"  
13 or "*nominally nonmagnetic*" [11,14], the PM phases are magnetically active in an external magnetic field as well  
14 as without field, developing small magnetic regions significantly above the Néel temperature.[9,12-14,38-41]  
15 This behavior was attributed to the spin-lattice coupling noted in the *spin-ordered AFM* phase based on the  
16 dependence of dielectric constant on the magnetic field[40] and DFT calculations of AFM-to-ferromagnetic  
17 transition on dielectric constant and phonon frequencies.[42] Whereas a similar scenario of spin-lattice coupling  
18 has also been suggested for the spin disordered PM phases[43] this is yet unclear given that the magnitude and  
19 distribution of the magnetic moments in the PM phases is unknown. As shown in Table I, provided one allows  
20 larger than conventional unit cells, the two PM phases are predicted by DFT to have a distribution of local  
21 magnetic moments of similar magnitude as the AFM phase.

22 (b) *Local structural symmetry breaking in the  $\gamma$  PM phase:* A recent analysis of the diffraction measured pair  
23 distribution function (PDF)[2] demonstrated that the nominally cubic  $\gamma$  phase manifests local octahedral tilting  
24 similar to those in low-temperature magnetically ordered tetragonal  $\alpha$  phase. This result thus demonstrates  
25 that the crystallographic structure of the  $\gamma$  PM phase is incompatible with the assigned nominal cubic Pm-3m  
26 symmetry having but a single octahedron per unit cell. In contrast, however, the PDF for the  $\beta$  PM phase at 100  
27 K can be explained with I4/mcm structure[2]. As Table I suggests, if the cubic  $\gamma$  PM phase is described by a larger  
28 than a conventional phase, DFT calculation predicts not only a distribution of local magnetic moments but also  
29 a distribution of lattice octahedral tilting.

30 The foregoing discussion suggests that a paramagnetic phase could manifest a distribution of (mutually  
31 compensating) local moments. In addition, if the PM is made of octahedra (as in perovskites) that can tilt, the  
32 PM phase can also manifest a distribution of local lattice tilting and distortions. Thus, depending on the phase,

1 the PM phase of perovskites can have both spin symmetry breaking as well as lattice symmetry breaking. This  
2 opens the door also for mutual coupling between spin and lattice. *Thus, paramagnetism and paraelasticity can*  
3 *coexist hand in hand as two forms of energy lowering local symmetry breaking.* Herein, we abandon the  
4 tradition of assigning *minimal monomorphous unit cell* having a single untitled octahedron and a single spin  
5 motif to describe a PM phase. We also avoid the harmonic phonon as a starting point of view for coupling, using  
6 instead a full Born-Oppenheimer surface without specializing to small deviations from the well minimum.  
7 Instead, we allow a larger cell where both positional and spin symmetry breaking lower the energy. We find  
8 that the  $\beta$  PM phase retains the positional minimal tetragonal  $I4/mcm$  cell (no formation of the structural  
9 polymorphous network characterized by the existence of a distribution of positional local motifs) but shows  
10 magnetic symmetry breaking, characteristic of a larger polymorphous *spin* unit cell with nonzero Eu local  
11 magnetic moments. In contrast, the  $\gamma$  PM phase must be described using polymorphous (pseudo) cubic network  
12 simultaneously accounting for both positional and spin-broken symmetries. These results obtained by  
13 minimization of the quantum mechanical forces with allowing for local magnetic moments to develop finite  
14 values subject to the zero global moment condition (see DFT details) explain why  $\beta$  and  $\gamma$  PM phases are  
15 magnetically active and why they have an intrinsic tendency for structural/spin symmetry breaking.

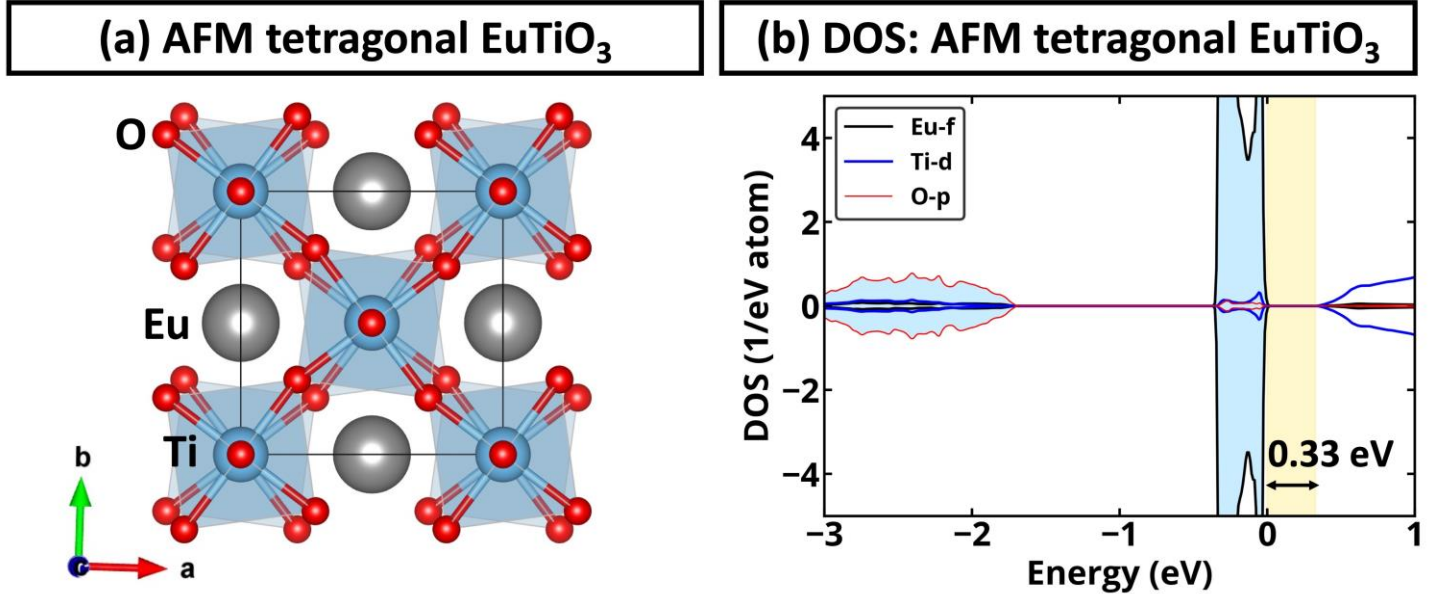
## 17 **II. Results and discussion**

### 18 **A. The $\alpha$ phase of $\text{EuTiO}_3$ : antiferromagnetic tetragonal insulator**

19 By screening the DFT calculated total energy of all unique magnetic configurations in tetragonal ETO supercells  
20 containing up to 8 formula units (fu), we identify that the  $\alpha$  phase is an antiferromagnetic (AFM-G) insulator, in  
21 agreement with experimental observations[7] and other first-principles calculations[44-48].

22 *Local moment and local octahedral tilting in the  $\alpha$  phase:* Figure 1a,b shows the crystal structure of the lowest  
23 energy AFM configuration of the  $\alpha$  phase of ETO and the DFT calculated density of states. In the AFM magnetic  
24 configuration, each Eu atom has a DFT magnetic moment of  $6.89\mu_B$ , while magnetic moments on Ti and O are  
25 zero within numerical precision. In the resulting structure, Ti atoms do not have any off-centered displacements  
26 and  $\text{TiO}_6$  octahedra exhibit  $a^0b^0c^-$  tilting (i.e.,  $R_5^-$  distortion mode of  $Pm-3m$  structure) with an amplitude of  $7.83^\circ$   
27 in agreement with that ( $\sim 7.5^\circ$ ) predicted by other first-principles calculations[44]. This tilting angle is  
28 overestimated as compared to  $3.53^\circ$  corresponding to the experimentally observed crystal structure (i.e.,  
29 experimental lattice vectors and Wyckoff positions) based on the Rietveld refinement against neutron powder  
30 diffraction data collected at 1.5 K[6]. The difference in rotation angle is not due to difference in lattice constants:  
31 the experimental lattice constants are  $a = 5.50$  and  $c = 7.80 \text{ \AA}$ [6], while the corresponding DFT (PBE+U) values

1 are  $a = 5.55$  and  $c = 7.94$  Å. When we use the experimental lattice constants rather than the DFT optimized value,  
 2 the tilting angle is 8.1 degrees. Hence, we surmise that the smaller measured tilting angle is associated with the  
 3 over localization of the Eu-4f electrons missed by DFT without good cancellation of the self-interaction energy.  
 4 This picture is confirmed by fact that the increase of U values results in approaching the DFT  $\text{TiO}_6$  tilting angle  
 5 towards the experimental value.[44]



6  
 7 **Figure 1. The  $\alpha$  phase of  $\text{EuTiO}_3$ : antiferromagnetic tetragonal insulator.** (a) Crystal structure of tetragonal  $\text{EuTiO}_3$ . (b) The orbital and  
 8 atom projected density of states (DOS) for AFM-G type tetragonal  $\text{EuTiO}_3$ . The occupied states are shadowed in light blue. The upper  
 9 valence band is Eu f-like, and the lower conduction bands are Ti-d like. The band gap region is shown in yellow. All results are presented  
 10 for PBE+U calculations with a U-J value of 5.2 eV applied on Eu-f states.

11  
 12 *Scenario of ferroelectricity in the  $\alpha$  phase:* Recently, the observation of soft phonons in the  $\alpha$  and  $\beta$  phases  
 13 [49,50] was interpreted as ferroelectric-like behavior (i.e., Ti-off centering)[50]. We note that DFT total energy  
 14 calculations[51] were shown to reliably and systematically predict which compounds are ferroelectric  
 15 compounds and which are not. Using the same DFT, we find no ferroelectric Ti displacements in the  $\alpha$  phase in  
 16 agreement with other first-principles simulations[42,44,45], and the crystallographic data identifying  
 17 centrosymmetric space group for the  $\alpha$  phase.[6] Recent experimental observation indicates that ETO is  
 18 ferroelectric only under strain.[42,52]

19 *Electronic structure of the  $\alpha$  phase:* The  $\alpha$  phase of  $\text{EuTiO}_3$  is an antiferromagnetic tetragonal insulator with  
 20 PBE+U band gap energy of 0.33 eV (underestimated as compared to the experimental value of  $\sim 0.8$ -1.3 eV  
 21 corresponding to the  $\beta$  and  $\gamma$  phases[15-17]). The upper valence band is composed of Eu-4f states with a minor  
 22 contribution of Ti-3d and O-2p states and is occupied by 7e per formula unit. The deeper valence band is located  
 23 at  $E_v - 2$  eV and is O-p like band. The conduction band is dominated by Ti-d states. Thus, the occupied narrow Eu-

1 4f band is an isolated impurity-like band nested within the bonding-antibonding Ti-O gap. This computed  
2 electronic structure thus sheds light on the possible reason behind the 4.53 eV transition (referenced as band  
3 gap energy) measured by spectroscopic ellipsometry at room temperature.[18] If the latter value corresponds  
4 to the minimum energy band gap then it contradicts existing theoretical and experimental literature on band  
5 gap energy of ETO phases. However, this value could correspond to the O-2p to Ti-3d transition as has been also  
6 suggested by the analysis of temperature-dependent optical absorption coefficient and its correlation to DFT  
7 electronic structure.[17] Thus, the above transition measured by spectroscopic ellipsometry need not  
8 correspond to the minimum energy gap.

9 One may wonder what is the impact of local structure on the electronic properties of ETO. To answer this  
10 question, we compare the band gap energies and total energies for AFM-G  $\alpha$  phase with fixed untilted (i.e., ideal  
11 cubic Pm-3m structure) and equilibrium tilting. It turns out that the band gap energy for the untilted AFM  $\alpha$   
12 phase is 0.37 eV, which is slightly larger than that (i.e., 0.33 eV) for the structure obtained by minimization of  
13 quantum forces. Here, however, the tilting is the energy lowering reaction resulting in reduction of internal  
14 energy by -5.4 meV/atom. These results thus show small variation of band gap energy with respect to local  
15 internal structure, which is mainly caused by the localization of Eu-4f states being rather unresponsive to TiO<sub>6</sub>  
16 octahedral tilting. We conclude that tilting stabilizes the AFM system while reducing the gap.

## 17 18 **B. The $\beta$ phase of EuTiO<sub>3</sub>: paramagnetic tetragonal insulator**

19 While the first-principles literature on ETO is rich of theoretical investigations of the magnetically ordered  $\alpha$ [44-  
20 48] or cubic (not experimentally existing phase) Pm-3m[15,42,53] phases, the PM tetragonal ETO phase has not  
21 been discussed in the theoretical literature. To assess the polymorphous picture of ETO and establish if the  
22 symmetry breaking is only in the geometric atomic distortions ("positional") and/or magnetic ("spin"), we design  
23 calculations that can reveal this. The first adapt the experimentally observed structural crystal structure with no  
24 spin symmetry breaking, while the second allows both positional and spin symmetry breaking.

### 25 **1. The $\beta$ PM phase of EuTiO<sub>3</sub> described with positional but not spin symmetry breaking**

26 Figure 2a,b shows for the  $\beta$  phase (computed using a tetragonal (I4/mcm) primitive cell containing two ABO<sub>3</sub>  
27 formula units) the electronic structure and magnetic properties in the spin symmetry unbroken (i.e.,  
28 nonmagnetic, non- spin-polarized) but positional symmetry broken description. While the main positional  
29 symmetry breaking is the R<sub>5</sub><sup>-</sup> distortion mode of Pm-3m as is the case for the  $\alpha$  AFM phase, due to nonmagnetic  
30 assumption and un-paired *f* electrons in NM ETO, each atom has zero magnetic moment (Fig. 2b). This thus  
31 results in a (false) metal (Fig. 2a). Similar to Mott insulators, due to odd number of electrons, splitting of Eu  
32 states cannot be done by positional symmetry breaking alone. This thus suggests that ignoring magnetic



1 symmetry breaking leads to the metallic state. This metallic electronic structure differs from that in typical  
2 monatomic metals (e.g., Cu or Al) in that the former has the Fermi level inside the principal conduction band  
3 but there is an internal wide band gap below the conduction band minimum (CBM) and above the deep valence  
4 band maximum (VBM) (see Fig. 2a). Compounds with such electronic structures can be thought of as  
5 "degenerate gapped metals".[54,55] In practice, they are often *False Metals* when the freedom to lower their  
6 energy by moving the Fermi level from the continuum into the principle VBM-CBM band gap region is not  
7 afforded in the calculation, as discussed in Ref.[26] Herein, we find that the symmetry unbroken nonmagnetic  
8 model results in DFT total energy that is 1.56 eV/atom above that of the  $\alpha$  phase. This energy difference is  
9 enormously large as compared to the typical energy difference between low- and high-temperature phases of  
10 different compounds (e.g., in order of a few meV/atom for typical nonmagnetic  $ABO_3$  perovskites[56,57]) clearly  
11 implying that the non-magnetic model is not a reasonable starting model.

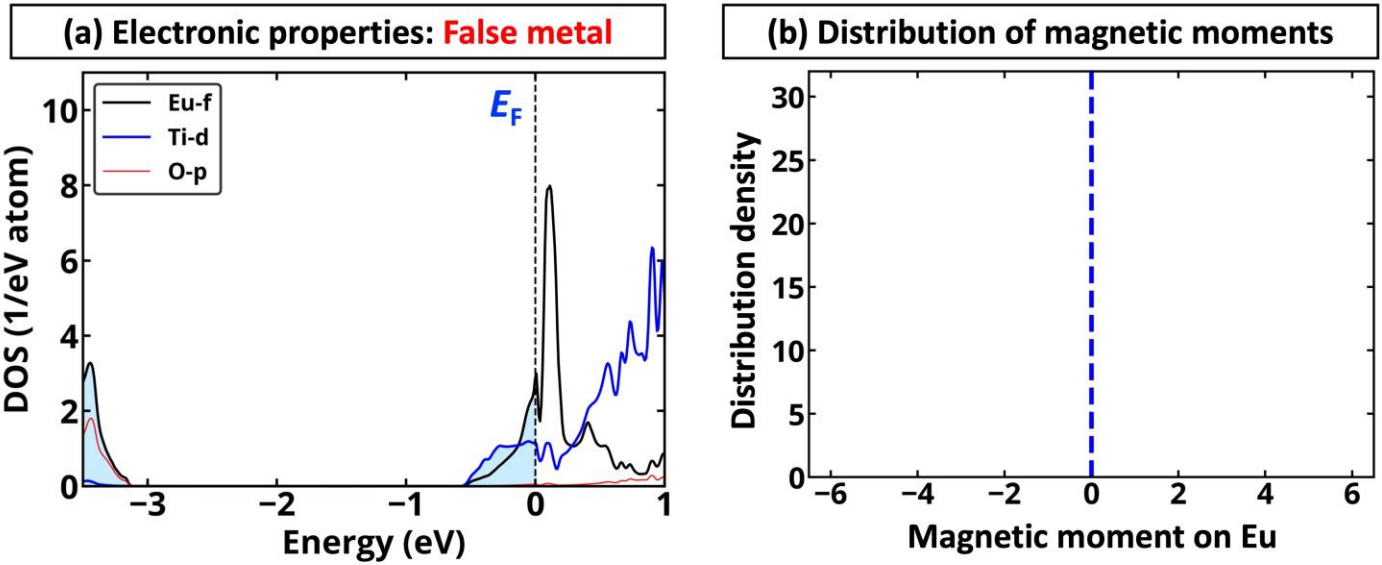
## 13 **2. The $\beta$ PM phase of $EuTiO_3$ described with both positional and spin symmetry breaking**

14 To describe the properties of the PM tetragonal phase, we adopt the recently proposed spin polymorphous  
15 model[25-30,58] allowing for positional and spin symmetry breaking. All calculations are performed using the  
16  $2 \times 2 \times 2$  supercell (32 fu/cell) of the conventional tetragonal  $I4/mcm$  structure. To allow for a local spin moment,  
17 we use the collinear magnetic calculations of special quasi-random structure (SQS)[37] (corresponding to the  
18 high temperature limit) where moments on Eu sites are oriented up or down. Although possible, there is no  
19 evidence to our knowledge that show non-collinear spin arrangement in the PM phases of ETO. We note  
20 however that such a non-collinear setup was recently used in simpler case of PM NiO[59], where the spin-spin  
21 SRO and direction of magnetic moments were calculated via the Heisenberg Monte-Carlo using DFT exchange  
22 energies and demonstrated comparable results to the collinear SQS calculations. To enable local positional  
23 symmetry breaking such as octahedral tilting, should it lower the energy, we minimize quantum mechanical  
24 forces while restricting the supercell shape to the global macroscopic tetragonal lattice (for the  $\gamma$  phase  
25 discussed below, the supercell shape is restricted to the global macroscopic cubic lattice) after introducing  
26 random atomic displacements for each atom with arbitrary direction and maximum displacement amplitude of  
27 0.1 Å.

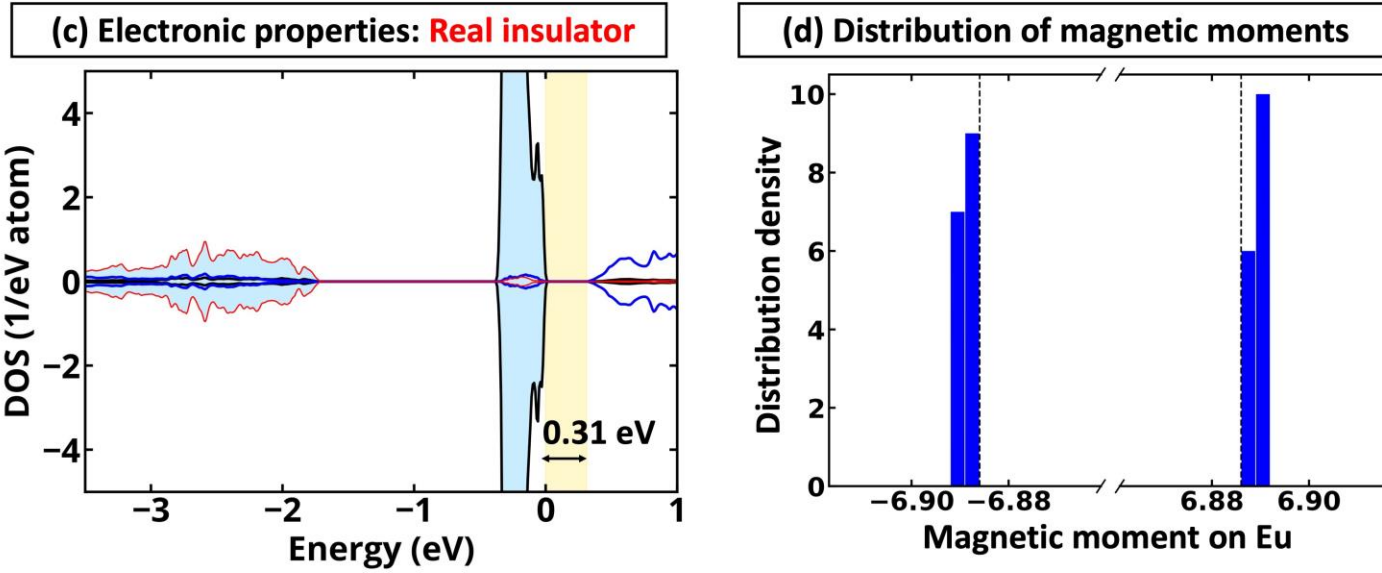
28 Figure 2c,d shows the results for the  $\beta$  phase allowing for both spin and structural symmetry breaking (i.e.,  
29 computed using the spin polymorphous model), demonstrating that the resulting system is a magnetic insulator  
30 with PBE+U band gap energy of 0.31 eV and internal DFT energy of over 1.56 eV/atom lower than that of the  
31 nonmagnetic symmetry unbroken model. Here, while the total magnetic moment is 0, there is a narrow  
32 distribution of local magnetic moments, i.e., each Eu site has an absolute local magnetic moment of

1 6.88±0.005μ. These results thus highlight the fundamental difference in the description of PM compounds with  
2 spin polymorphous model and nonmagnetic approach, demonstrating that accounting for a spin and structural  
3 symmetry breaking can allow describing gapping in the β phase. Moreover, since each site in such PM tetragonal  
4 ETO structure has a local magnetic moment, it is not surprising that the β phase is magnetically active and  
5 responds to the magnetic field. While breaking the spin symmetry results in coupling to local structural  
6 symmetry breaking, for the β phase, such coupling is extremely weak and maximum Eu and Ti atomic  
7 displacements are less than 0.001 Å (i.e., numerically zero) with respect to their ideal Wyckoff positions.  
8 Breaking of local spin symmetry does not result in a significant change of local octahedral tilting as well – the  
9 amplitude of a<sup>0</sup>b<sup>0</sup>c<sup>-</sup> tilting is 8.01±0.02°, which is close to the value given above for the α phase (this angle is  
10 overestimated as compared to experimental studies as noted above). We still identify the R<sub>5</sub><sup>-</sup> distortion mode  
11 as the main symmetry breaking present in the β phase in spin polymorphous calculations. To estimate the  
12 relative contribution ( $I_k$ ) of the R<sub>5</sub><sup>-</sup> distortion mode to symmetry breaking in the β phase, we calculate  $I_k =$   
13  $\frac{A_k}{\sum_i^N A_i}$ , where  $A_i$  is the amplitude of  $i$  symmetry breaking mode observed in the system among N observed modes.  
14 The computed results suggest that the relative contribution of R<sub>5</sub><sup>-</sup> distortion mode is 99%, which is consistent  
15 with the fact that experimentally the β phase is known to have the I4/mcm symmetry without distinct structural  
16 symmetry breaking as confirmed by experimental measurements of the pair distribution function.[2] These  
17 results imply that spin-symmetry breaking causes the band gap opening in the β phase, while the structural  
18 symmetry breaking is the energy lowering reaction. This is in good agreement with the fact that SQS calculations  
19 applied on frozen tetragonal structure (i.e., that obtained for the α phase) result in band gap energy of 0.31 eV  
20 and internal energy only 0.02 meV/atom higher than that found in the corresponding calculations with allowed  
21 structural symmetry breaking.

**Nonmagnetic symmetry unbroken approximation of PM EuTiO<sub>3</sub> ( $\beta$  phase)**  
 $\Delta E = 1561$  meV/atom;  $R_5^-$  mode contribution = 100%



**Spin polymorphous symmetry broken approximation of PM EuTiO<sub>3</sub> ( $\beta$  phase)**  
 $\Delta E = 0.18$  meV/atom;  $R_5^-$  mode contribution = 99%



1  
2  
3  
4  
5  
6  
7  
8  
9  
10  
11

**Figure 2. The  $\beta$  phase of EuTiO<sub>3</sub>: paramagnetic tetragonal insulator.** (a,c) Electronic and (b,d) magnetic properties of the paramagnetic  $\beta$  phase of EuTiO<sub>3</sub> computed for (a,b) nonmagnetic symmetry-unbroken model and (c,d) spin polymorphous symmetry-broken model. Spin polymorphous symmetry-broken model is reproduced by the nudging of 160-atom SQS supercell of tetragonal EuTiO<sub>3</sub> allowing internal relaxation and volume optimization but keeping tetragonal lattice vectors. The band gap region in (c) is shown in yellow. The dashed black line in (d) shows the magnetic moments in the  $\alpha$  AFM phase. The contribution of different modes to symmetry breaking in the paramagnetic  $\beta$  phase is computed as  $I_k = \frac{A_k}{\sum_i^N A_i}$ , where  $A_i$  is the amplitude of  $i$  symmetry breaking mode observed in the system, and  $N$  is the number of symmetry-breaking modes present in the system with respect to Pm-3m structure. The internal energy is given with respect to AFM-G tetragonal EuTiO<sub>3</sub>. All results are presented for PBE+U calculations with a U-J value of 5.2 eV applied on Eu-f states.

## C. The $\gamma$ PM phase of $\text{EuTiO}_3$ : paramagnetic cubic insulator

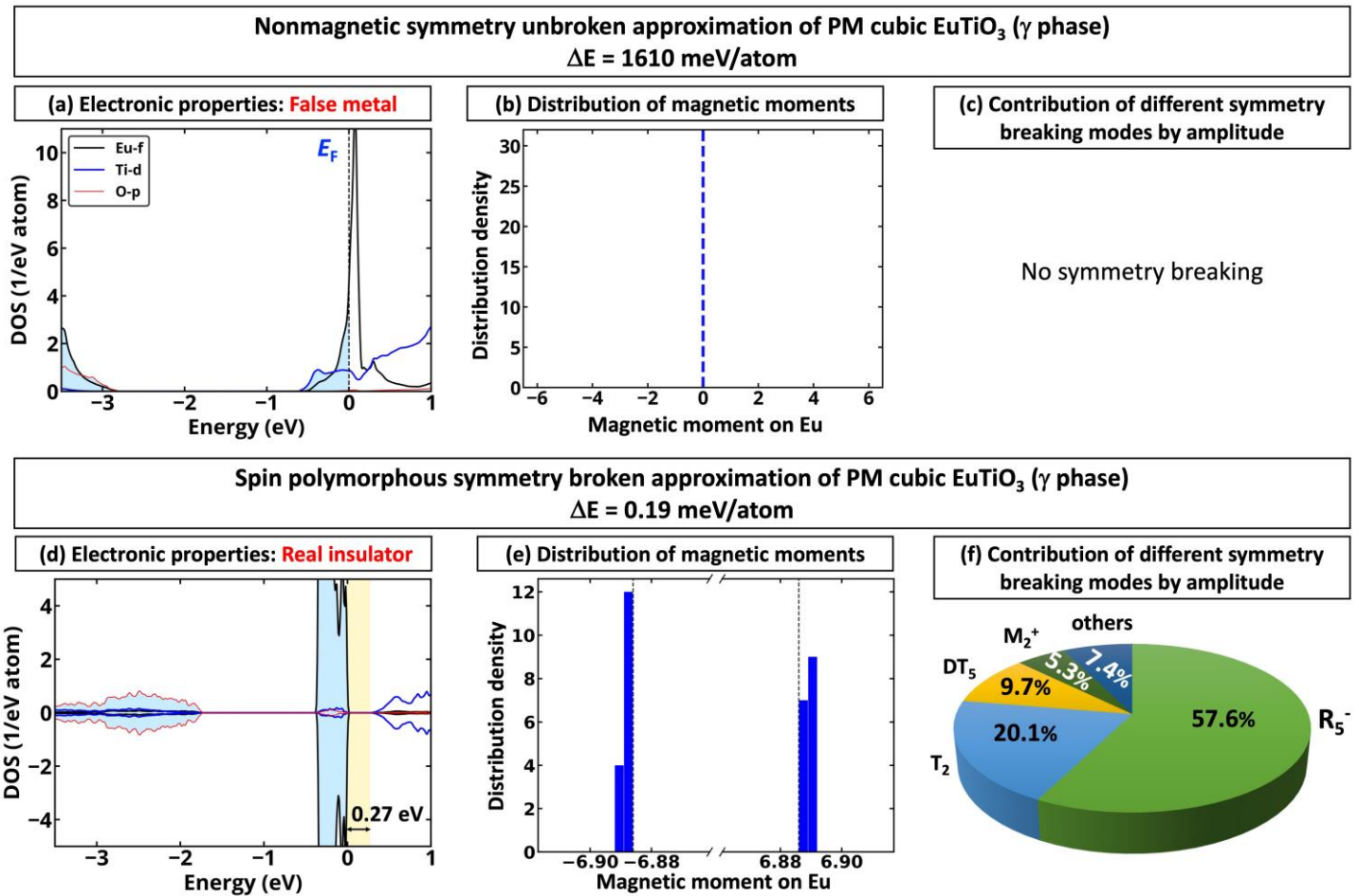
### 1. *The $\gamma$ PM phase of $\text{EuTiO}_3$ described with positional and spin unbroken symmetry*

Figure 3a-c shows the results for electronic, magnetic, and symmetry for a nonmagnetic description of the  $\gamma$  PM phase. Similar to the case of the  $\beta$  phase, nonmagnetic (symmetry unbroken) approximation of the  $\gamma$  phase results in a degenerate gapped metal with Fermi level in the conduction band (Fig. 3a), which is in contradiction with the experimental observation of an insulating state for the  $\gamma$  phase (see Table 1). The energy of nonmagnetic cubic ETO is 1.61 eV/atom above that for the ground state structure ( $\alpha$  phase), i.e., it lies extremely in high energy and therefore unlikely to be of physical importance. Moreover, similar to the  $\beta$  phase, zero magnetic moment on each atom (Fig. 3b) of the monomorphous nonmagnetic system cannot explain why the  $\gamma$  PM phase is magnetically active above the Néel temperature.[9,12-14,38-40] Finally, such a model (Fig. 3c) does not allow to explain why the experimental pair distribution function revealed that the  $\gamma$  phase exists as the symmetry-broken structure with local structural motifs of the  $\alpha$  phase.[2]

### 2. *The $\gamma$ PM phase of $\text{EuTiO}_3$ described with both positional and spin symmetry breaking*

Figure 3d-f shows the results of the application of the spin polymorphous model to  $2\sqrt{2}\times 2\sqrt{2}\times 4$  supercell (32fu/cell) of nominal Pm-3m ETO structure. In contrast to the nonmagnetic monomorphous approximation of the  $\gamma$  PM phase, allowing spin and structural symmetry breaking results in a structural and spin polymorphous system with the PBE+U band gap energy of 0.27 eV (Fig. 3d) and a distribution of local magnetic and structural motifs (Fig. 3e,f). First, while the total magnetic moment of the cell is 0, the Eu sublattice has a small distribution of local magnetic motifs on Eu atoms with an average absolute value of the magnetic moment of  $6.88\pm 0.005\mu_B$ . These results thus suggest that spin polymorphism does not result in substantial distribution of local magnetic moments on magnetic species, however, this is not always the case for PM compounds. For instance, PM monoclinic  $\text{YNiO}_3$ [60] and PM tetragonal  $\text{FeSe}$ [61] have a significantly larger variation of magnetic moments on metal sublattices. The obtained local moments on each Eu ion thus clearly implies that the  $\gamma$  phase is magnetically active, which is in agreement with experimental observations.[9,12-14,38-40] Second, the resulting structure has different structural motifs (see Fig. S1): there are (i) distribution of small atomic displacements for Eu and Ti atoms and (ii) distribution of octahedral tilting as compared to the ideal monomorphous Pm-3m ETO structure. While the maximum Eu and Ti displacements in the structure are 0.08 and 0.03 Å, respectively, the maximum averaged displacement (i.e.,  $\langle x \rangle = \frac{1}{N} \sum_{i=0}^N x_i$ , where N is a number of corresponding atoms) along a, b, and c axis for Eu and Ti atoms is less than 0.001 Å for a 160-atom cell. To further understand the relation of the symmetry breaking observed in the spin polymorphous model, we apply

1 the analysis of local structural symmetry-breaking modes as compared to the monomorphous Pm-3m structure.  
2 The results are summarized in Fig. 3f, showing that: (i) the  $\gamma$  phase exhibits the distribution of different structural  
3 symmetry-breaking modes as compared to Pm-3m structure; (ii) the main dominant mode corresponds to  $R_5^-$ ,  
4 which is the same as that present in the AFM tetragonal  $\alpha$  phase, (iii)  $T_2$ ,  $DT_5$ , and  $M_5^+$  are other symmetry-  
5 breaking modes with noticeable amplitude observed in the polymorphous structure. These data thus confirm  
6 that PM cubic ETO structure tends to minimize the energy by structural symmetry breaking adapting the motifs  
7 (i.e.,  $R_5^-$  distortion) of the low-temperature  $\alpha$  phase, which is in good agreement with results predicted based  
8 on the analysis of the diffraction measured pair distribution function[2]. We note that similar to the  $\alpha$  and  $\beta$   
9 phases, accounting of structural distortions is not necessary for prediction of insulation state of  $\gamma$  phase but is  
10 essential for accurate prediction of band gap energy. Thus, while nonmagnetic frozen cubic ETO structure is  
11 metallic with high internal energy of 1.61 eV/atom (with respect to ground state structure), spin SQS calculations  
12 for frozen cubic internal structure result in insulator with band gap energies of 0.36 eV and relative internal  
13 energies of 5.3 meV/atom. Allowing structural distortion in spin SQS calculations further reduces the internal  
14 energy to 0.2 meV/atom causing the reduction of band gap energy to 0.27 eV. These results thus also conclude  
15 that *the*  $\gamma$  phase cannot be described as ideal high-symmetry cubic perovskite structure and indeed exhibit both  
16 structural and spin m-DOFs, which only can be captured using a non-trivial supercell allowing for spin and  
17 structural symmetry breaking.



**Figure 3. The  $\gamma$  phase of EuTiO<sub>3</sub>: paramagnetic cubic insulator.** (a,d) Electronic, (b,e) magnetic, and (c,f) structural properties of paramagnetic  $\gamma$  phase of EuTiO<sub>3</sub> computed for (a-c) nonmagnetic symmetry-unbroken model and (d-f) spin polymorphous symmetry-broken model. The spin polymorphous symmetry-broken structure is obtained by the nudging of 160-atom SQS supercell of cubic EuTiO<sub>3</sub> allowing internal relaxation and volume optimization but keeping cubic lattice vectors. The band gap region in (d) is shown in yellow. The dashed black line in (e) shows the magnetic moments in the  $\alpha$  phase. Contribution of different modes to symmetry breaking in paramagnetic  $\gamma$  phase is computed as  $I_k = \frac{A_k}{\sum_i^N A_i}$ , where  $A_i$  is the amplitude of  $i$  symmetry breaking mode observed in the system, and  $N$  is the number of symmetry-breaking modes present in the system with respect to Pm-3m structure. The internal energy is given with respect to AFM-G tetragonal EuTiO<sub>3</sub>. All results are presented for PBE+U calculations with U-J value of 5.2 eV applied on Eu-f states.

### III. Conclusions

Allowing for the existence of different *structural local motifs* (rotated, tilted, deformed or disproportionated BO<sub>6</sub> octahedra) and *spin local motifs*, we demonstrate that  $\alpha$ ,  $\beta$ , and  $\gamma$  phases of ETO develop different degrees of symmetry breaking. At low temperatures, the  $\alpha$  phase - magnetically ordered AFM tetragonal ETO is an insulator that exhibits  $R_5^-$  ordered distortion with respect to the Pm-3m structure and each Eu atom having the same magnetic moments. This  $\alpha$  phase can be described using a small primitive cell containing only 4 fu

1 accounting for a single distortion mode. The  $\beta$  phase is a PM tetragonal insulator that is spin polymorphous and  
2 exhibits magnetic symmetry breaking with each Eu atom being magnetically unique and having its local magnetic  
3 moment. The accurate description of this phase (as well as  $\gamma$  phase) requires using large supercell with allowing  
4 spin symmetry breaking (e.g., via employing special quasi-random structure spin distribution). In the resulting  
5 symmetry broken structure, the  $\beta$  phase still exhibits the  $R_5^-$  distortion but does not have other noticeable  
6 structural symmetry breaking modes. The high-temperature PM cubic  $\text{EuTiO}_3$  ( $\gamma$  phase) is a polymorphous  
7 insulator that exhibits both structural and magnetic symmetry breaking as a result of internal energy  
8 minimization. The  $\gamma$  phase has the distribution of both local spin and structural motifs. Here, the  $R_5^-$  distortion  
9 remains the main structural symmetry-breaking mode, suggesting that the internal structure of the  $\gamma$  phase  
10 mimics the distortion observed in the  $\alpha$  phase, with some contribution of other symmetry breaking modes that  
11 are not present in the low-temperature  $\alpha$  phase, which is in good agreement with experimental results.  
12 Importantly, we demonstrate that in properly described PM  $\beta$  and  $\gamma$  phases, each Eu atom has local magnetic  
13 moments, consistent with the observation of local magnetic activity in  $\text{EuTiO}_3$  significantly above the Néel  
14 temperature. These results thus imply that magnetic field dependence of  $\beta$ - $\gamma$  transition temperature is likely  
15 caused by difference in response of local spin environments in  $\beta$  and  $\gamma$  phases to the magnetic field, which  
16 however will require more detailed future investigation.

17  
18 **Acknowledgment:** U.S. Department of Energy, Office of Science, Basic Energy Sciences, Materials Sciences and  
19 Engineering Division within DE-SC0010467 support this work. The authors acknowledge the use of Extreme  
20 Science and Engineering Discovery Environment (XSEDE) supercomputer resources, which are supported by the  
21 National Science Foundation, grant number ACI-1548562.

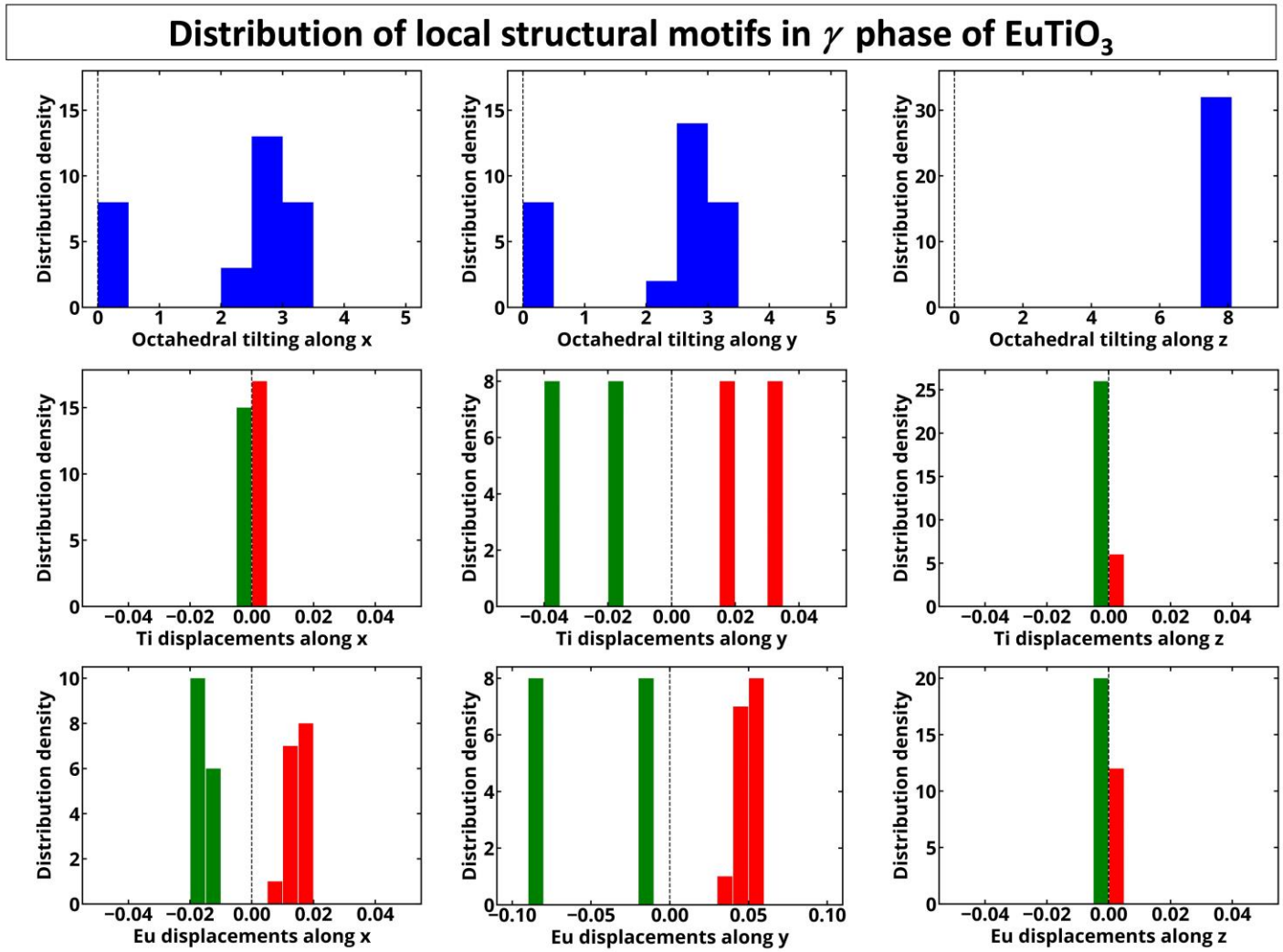
## 22 23 **APPENDIX: DFT details**

24 The first-principles calculations are performed using pseudopotential plane-wave DFT as implemented in the  
25 Vienna Ab Initio Simulation Package (VASP)[62-64] with Perdew-Burke-Ernzerhof (PBE)[65] exchange-  
26 correlation functional and +U correction (U-J value of 5.2 eV) introduced by Dudarev et al.[66] applied on Eu-f  
27 states. The cutoff energies for the plane-wave basis are set to 500 eV for final calculations and 550 eV for volume  
28 relaxation. Atomic relaxations are performed until the internal forces are smaller than 0.01 eV/Å, unless  
29 specified. To identify the main the symmetry-breaking modes in each phase, we employed the  
30 AMPLIMODES[67,68] and ISOTROPY[69,70] that allow identifying the symmetry-breaking modes in the  
31 compound via generating atomic displacement patterns induced by irreducible representations of the parent  
32 (i.e., Pm-3m in this work) space-group symmetry. We note that for non-magnetic  $\beta$  and  $\gamma$  phase calculations,

1 the results are presented for lowest energy configurations obtained by occupation matrix (25 occupation matrix  
 2 were tested for each system) control using the method proposed by Allen and Watson.[71]

3

4 **APPENDIX: Distribution of local structural motifs in the  $\gamma$  phase of  $\text{EuTiO}_3$  as computed using the spin**  
 5 **polymorphous model**



6

7 **Figure S1.** Distribution of local structural motifs in spin and structural polymorphous cubic  $\text{EuTiO}_3$  shown as distribution of octahedral  
 8 tilting, Eu displacements, and Ti displacements. The maximum averaged displacement (e.g.,  $\langle x \rangle = \frac{1}{N} \sum_{i=0}^N x_i$ , where N is number of  
 9 corresponding atoms) along x, y, and z axis for Eu and Ti atoms is less than 0.001 Å for 160-atom cell. Corresponding tilting angles and  
 10 Eu/Ti atomic displacements in monomorphous cell are shown by dashed line.

11

12 **References:**

13 [1] V. Goian, S. Kamba, O. Pacherová, J. Drahokoupil, L. Palatinus, M. Dušek, J. Rohlíček, M. Savinov, F.  
 14 Laufek, W. Schranz, A. Fuith, M. Kachlák, K. Maca, A. Shkabko, L. Sagarna, A. Weidenkaff, and A. A. Belik,  
 15 Phys. Rev. B, **86**, 054112 (2012).  
 16 [2] M. Allieta, M. Scavini, L. J. Spalek, V. Scagnoli, H. C. Walker, C. Panagopoulos, S. S. Saxena, T.  
 17 Katsufuji, and C. Mazzoli, Phys. Rev. B, **85**, 184107 (2012).



- [3] J. Köhler, R. Dinnebier, and A. Bussmann-Holder, *Phase Transitions*, **85**, 949 (2012).
- [4] P. Parisiades, E. Liarokapis, J. Köhler, A. Bussmann-Holder, and M. Mezouar, *Phys. Rev. B*, **92**, 064102 (2015).
- [5] D. S. Ellis, H. Uchiyama, S. Tsutsui, K. Sugimoto, K. Kato, D. Ishikawa, and A. Q. R. Baron, *Phys. Rev. B*, **86**, 220301 (2012).
- [6] B. J. Kennedy, G. Murphy, E. Reynolds, M. Avdeev, H. E. R. Brand, and T. Kolodiazny, *J. Phys.: Condens. Matter*, **26**, 495901 (2014).
- [7] T. R. McGuire, M. W. Shafer, R. J. Joenk, H. A. Alperin, and S. J. Pickart, *J. Appl. Phys.*, **37**, 981 (1966).
- [8] D. Bessas, K. Z. Rushchanskii, M. Kachlik, S. Disch, O. Gourdon, J. Bednarcik, K. Maca, I. Sergueev, S. Kamba, M. Ležaić, and R. P. Hermann, *Phys. Rev. B*, **88**, 144308 (2013).
- [9] P. Pappas, M. Calamiotou, M. Polentarutti, G. Bais, A. Bussmann-Holder, and E. Liarokapis, arXiv:2103.04742 [cond-mat], (2021).
- [10] A. Bussmann-Holder, J. Köhler, R. K. Kremer, and J. M. Law, *Phys. Rev. B*, **83**, 212102 (2011).
- [11] A. Bussmann-Holder, K. Roleder, B. Stuhlhofer, G. Logvenov, I. Lazar, A. Soszyński, J. Koperski, A. Simon, and J. Köhler, *Sci. Rep.*, **7**, 40621 (2017).
- [12] A. Bussmann-Holder, J. Köhler, K. Roleder, Z. Guguchia, and H. Keller, *Thin Solid Films*, **643**, 3 (2017).
- [13] Z. Guguchia, Z. Salman, H. Keller, K. Roleder, J. Köhler, and A. Bussmann-Holder, *Phys. Rev. B*, **94**, 220406 (2016).
- [14] G. Gregori, J. Köhler, J. F. Scott, and A. Bussmann-Holder, *J. Phys.: Condens. Matter*, **27**, 496003 (2015).
- [15] H. Akamatsu, K. Fujita, H. Hayashi, T. Kawamoto, Y. Kumagai, Y. Zong, K. Iwata, F. Oba, I. Tanaka, and K. Tanaka, *Inorg. Chem.*, **51**, 4560 (2012).
- [16] J. H. Lee, X. Ke, N. J. Podraza, L. F. Kourkoutis, T. Heeg, M. Roeckerath, J. W. Freeland, C. J. Fennie, J. Schubert, D. A. Muller, P. Schiffer, and D. G. Schlom, *Appl. Phys. Lett.*, **94**, 212509 (2009).
- [17] K. Jiang, R. Zhao, P. Zhang, Q. Deng, J. Zhang, W. Li, Z. Hu, H. Yang, and J. Chu, *Phys. Chem. Chem. Phys.*, **17**, 31618 (2015).
- [18] B. Stuhlhofer, G. Logvenov, M. Górný, K. Roleder, A. Boris, D. Pröpper, R. K. Kremer, J. Köhler, and A. Bussmann-Holder, *Phase Transitions*, **89**, 731 (2016).
- [19] L. Zhang, Y. J. Zhou, L. Guo, W. W. Zhao, A. Barnes, H. T. Zhang, C. Eaton, Y. X. Zheng, M. Brahlek, H. F. Haneef, N. J. Podraza, M. H. W. Chan, V. Gopalan, K. M. Rabe, and R. Engel-Herbert, *Nat. Mater.*, **15**, 204 (2016).
- [20] F. Iori, M. Gatti, and A. Rubio, *Phys. Rev. B*, **85**, 115129 (2012).
- [21] E. Pavarini, S. Biermann, A. Poteryaev, A. I. Lichtenstein, A. Georges, and O. K. Andersen, *Phys. Rev. Lett.*, **92**, 176403 (2004).
- [22] M. G. Vergniory, L. Elcoro, C. Felser, N. Regnault, B. A. Bernevig, and Z. Wang, *Nature*, **566**, 480 (2019).
- [23] N. F. Mott and Z. Zinamon, *Rep. Prog. Phys.*, **33**, 881 (1970).
- [24] N. Mott, *Metal-insulator transitions* (CRC Press, London, 1990).
- [25] Z. Wang, O. I. Malyi, X. Zhao, and A. Zunger, *Phys. Rev. B*, **103** 165110 (2021).
- [26] O. I. Malyi and A. Zunger, *Appl. Phys. Rev.*, **7**, 041310 (2020).
- [27] J. Varignon, M. Bibes, and A. Zunger, *Nat. Commun.*, **10**, 1658 (2019).
- [28] J. Varignon, M. Bibes, and A. Zunger, *Phys. Rev. B*, **100**, 035119 (2019).
- [29] G. Trimarchi, Z. Wang, and A. Zunger, *Phys. Rev. B*, **97**, 035107 (2018).
- [30] Y. Zhang, J. Furnes, R. Zhang, Z. Wang, A. Zunger, and J. Sun, *Phys. Rev. B*, **102**, 045112 (2020).
- [31] H. Hasegawa, *J. Phys. Soc. Jpn.*, **46**, 1504 (1979).
- [32] J. Hubbard, *Phys. Rev. B*, **19**, 2626 (1979).
- [33] J. Hubbard, *Phys. Rev. B*, **20**, 4584 (1979).
- [34] B. Gyorffy, A. Pindor, J. Staunton, G. Stocks, and H. Winter, *Journal of Physics F: Metal Physics*, **15**, 1337 (1985).
- [35] R. Magri, S. H. Wei, and A. Zunger, *Phys. Rev. B*, **42**, 11388 (1990).
- [36] Z. W. Lu, S. H. Wei, and A. Zunger, *Phys. Rev. B*, **44**, 10470 (1991).
- [37] A. Zunger, S. H. Wei, L. G. Ferreira, and J. E. Bernard, *Phys. Rev. Lett.*, **65**, 353 (1990).

- 1 [38] Z. Guguchia, H. Keller, R. K. Kremer, J. Köhler, H. Luetkens, T. Goko, A. Amato, and A. Bussmann-  
2 Holder, *Phys. Rev. B*, **90**, 064413 (2014).
- 3 [39] Z. Guguchia, H. Keller, J. Köhler, and A. Bussmann-Holder, *J. Phys.: Condens. Matter*, **24**, 492201  
4 (2012).
- 5 [40] T. Katsufuji and H. Takagi, *Phys. Rev. B*, **64**, 054415 (2001).
- 6 [41] A. Bussmann-Holder, Z. Guguchia, J. Köhler, H. Keller, A. Shengelaya, and A. R. Bishop, *New J. Phys.*,  
7 **14**, 093013 (2012).
- 8 [42] C. J. Fennie and K. M. Rabe, *Phys. Rev. Lett.*, **97**, 267602 (2006).
- 9 [43] K. Caslin, R. K. Kremer, Z. Guguchia, H. Keller, J. Köhler, and A. Bussmann-Holder, *J. Phys.: Condens.*  
10 *Matter*, **26**, 022202 (2014).
- 11 [44] T. Birol and C. J. Fennie, *Phys. Rev. B*, **88**, 094103 (2013).
- 12 [45] K. Z. Rushchanskii, N. A. Spaldin, and M. Ležaić, *Phys. Rev. B*, **85**, 104109 (2012).
- 13 [46] Z. Gui and A. Janotti, *Phys. Rev. Lett.*, **123**, 127201 (2019).
- 14 [47] Y. Yang, W. Ren, D. Wang, and L. Bellaiche, *Phys. Rev. Lett.*, **109**, 267602 (2012).
- 15 [48] H. Akamatsu, Y. Kumagai, F. Oba, K. Fujita, K. Tanaka, and I. Tanaka, *Adv. Funct. Mater.*, **23**, 1864  
16 (2013).
- 17 [49] S. Kamba, D. Nuzhnyy, P. Vaněk, M. Savinov, K. Knížek, Z. Shen, E. Šantavá, K. Maca, M. Sadowski,  
18 and J. Petzelt, *Europhys. Lett.*, **80**, 27002 (2007).
- 19 [50] V. Goian, S. Kamba, J. Hlinka, P. Vaněk, A. A. Belik, T. Kolodiaznyy, and J. Petzelt, *The European*  
20 *Physical Journal B*, **71**, 429 (2009).
- 21 [51] C. M. Acosta, A. Fazzio, G. M. Dalpian, and A. Zunger, *Phys. Rev. B*, **102**, 144106 (2020).
- 22 [52] J. H. Lee, L. Fang, E. Vlahos, X. Ke, Y. W. Jung, L. F. Kourkoutis, J.-W. Kim, P. J. Ryan, T. Heeg, M.  
23 Roeckerath, V. Goian, M. Bernhagen, R. Uecker, P. C. Hammel, K. M. Rabe, S. Kamba, J. Schubert, J. W.  
24 Freeland, D. A. Muller, C. J. Fennie, P. Schiffer, V. Gopalan, E. Johnston-Halperin, and D. G. Schlom, *Nature*,  
25 **466**, 954 (2010).
- 26 [53] R. Ranjan, H. Sadat Nabi, and R. Pentcheva, *J. Phys.: Condens. Matter*, **19**, 406217 (2007).
- 27 [54] O. I. Malyi, M. T. Yeung, K. R. Poeppelmeier, C. Persson, and A. Zunger, *Matter*, **1**, 280 (2019).
- 28 [55] X. Zhang, L. Zhang, J. D. Perkins, and A. Zunger, *Phys. Rev. Lett.*, **115**, 176602 (2015).
- 29 [56] A. Jain, S. P. Ong, G. Hautier, W. Chen, W. D. Richards, S. Dacek, S. Cholia, D. Gunter, D. Skinner, G.  
30 Ceder, and K. A. Persson, *APL Mat.*, **1**, 011002 (2013).
- 31 [57] J. E. Saal, S. Kirklin, M. Aykol, B. Meredig, and C. Wolverton, *JOM*, **65**, 1501 (2013).
- 32 [58] Z. Wang, Q. Liu, J.-W. Luo, and A. Zunger, *Mater. Horiz.*, **6**, 2124 (2019).
- 33 [59] D. Gambino, O. I. Malyi, Z. Wang, B. Alling, and A. Zunger, (unpublished), (2021).
- 34 [60] A. Zunger and O. I. Malyi, *Chem. Rev.*, **121**, 3031 (2021).
- 35 [61] Z. Wang, X. Zhao, R. Koch, S. J. L. Billinge, and A. Zunger, *Phys. Rev. B*, **102**, 235121 (2020).
- 36 [62] G. Kresse and J. Hafner, *Phys. Rev. B*, **47**, 558 (1993).
- 37 [63] G. Kresse and J. Furthmüller, *Comp. Mater. Sci.*, **6**, 15 (1996).
- 38 [64] G. Kresse and J. Furthmüller, *Phys. Rev. B*, **54**, 11169 (1996).
- 39 [65] J. P. Perdew, K. Burke, and M. Ernzerhof, *Phys. Rev. Lett.*, **77**, 3865 (1996).
- 40 [66] S. L. Dudarev, G. A. Botton, S. Y. Savrasov, C. J. Humphreys, and A. P. Sutton, *Phys. Rev. B*, **57**, 1505  
41 (1998).
- 42 [67] J. Perez-Mato, D. Orobengoa, and M. Aroyo, *Acta Crystallogr. Sect. A: Found. Crystallogr.*, **66**, 558  
43 (2010).
- 44 [68] D. Orobengoa, C. Capillas, M. I. Aroyo, and J. M. Perez-Mato, *J. Appl. Crystallogr.*, **42**, 820 (2009).
- 45 [69] D. M. H. H. T. Stokes, and B. J. Campbell ISOTROPY Software Suite, [iso.byu.edu](http://iso.byu.edu).
- 46 [70] B. J. Campbell, H. T. Stokes, D. E. Tanner, and D. M. Hatch, *J. Appl. Crystallogr.*, **39**, 607 (2006).
- 47 [71] J. P. Allen and G. W. Watson, *Phys. Chem. Chem. Phys.*, **16**, 21016 (2014).
- 48